NEU PRESS

ASREL Aerospace Research Letters

Cilt: 4 Sayı: 2 Yıl: 2025 | Araştırma Makalesi | e-ISSN: 2980-0064

Design and Longitudinal Stability Analysis of a Stealth Unmanned Aerial Vehicle

Zekiye ÇİNAR[1] Rabia UZUN[1*] Tolunay DAĞ[1] Tuğrul OKTAY[2]

[1] Iskenderun Technical University, Faculty of Aerospace Sciences, Aerospace Engineering, Hatay, Türkiye

[2] Erciyes University, Faculty of Aviation and Space Sciences, Aircraft Engineering, Kayseri, Türkiye

Article Info

Received: 26.08.2025
Accepted: 21.10.2025
Published: 31.12.2025

Keywords:
UAV,
Fixed Wing,
Stealth Technology,
Longitudinal Stability.

ABSTRACT

This study includes the design and investigation stability of aircraft. The designed unnamed air vehicle (UAV) mission is conducting observation and gather intelligence without being detected by enemy radars. The designed UAV has fixed wing, mass of 10 kg and cruising speed of 30 m/s. The most important characteristic of UAV is use stealth technology.To select using stealth technology for UAV because the detection of UAVs using stealth technology is more difficult than that of conventional UAVs. When design, the initially selected wings profile analyzed use XFLR5 software. After choose S1210 airfoil profile among the other airfoils. Because S1210 airfoil profile has the best lift coefficient and minimum drag coefficient. The tail airfoil profile uses symmetric airfoil NACA 0010 because appropriate of aircraft design. Then selected profile, configuration selection phase exists. At this phase configuration selection for wing, fuselage, tail and landing gear. Mid-wing and T-tail configurations are used because they provide the aircraft with better balance and stability. Conventional fuselage and articulated landing gear configurations are used because they provide the aircraft minimum parasite drag and undetected by enemy radars. Then selected configuration, designed aerodynamic and control surface with specific dimensions and after the aircraft has been drafted using CAD software. Payload consists of T-Motor MN4014 brushless motor, compatible 40A ESC, 4S 5000mAh Li-Po battery, and Teledyne FLIR Hadron 640 imaging system for day and night reconnaissance missions. Then design phase, state-space matrices has been created because aircraft designed to investigate longitudinal stability. In the matrix parameters used to XFLR5 software derived from the stability of analysis and elevator deflection is OpenVSP software derived from the analysis. The finally, PID controller used for investigation stability and the best system's response was derived.

Hayalet İnsansız Hava Aracının Tasarımı ve Boylamasına Kararlılığının İncelenmesi

Makale Bilgisi

Geliş Tarihi: 26.08.2025
Kabul Tarihi: 21.10.2025
Yayın Tarihi: 31.12.2025

Keywords:
İHA,
Sabit Kanat,
Gizlilik Teknolojisi,
Boylamasına Kararlılık.

ÖZET

Bu çalışma, görevi düşman radarlarına yakalanmadan gözlem yaparak bilgi toplamak olan insansız hava aracının tasarımını ve kararlılığının incelenmesini içermektedir. Tasarlanan hava aracı, sabit kanatlı, 10 kg ağırlığında ve 30 m/s seyir hızına sahiptir. Ayrıca hava aracının en önemli özelliği gizlilik teknolojisini kullanıyor olmasıdır. Gizlilik teknolojisine sahip insansız hava araçlarının geleneksel hava araçlarına göre tespit edilmesi daha zor olduğu için bu görev türünde tercih edilmiştir. Tasarım aşamasında ilk olarak belirlenen kanat profillerinin XFLR5 programında analizleri gerçekleştirilmiş ve kriterlere göre değerlendirilerek en iyi taşıma katsayısına ve minimum sürüklemeye sahip S1210 kanat profili seçilmiştir. Hava aracı tasarımına uygun olması nedeniyle kuyruk profilinde simetrik bir profil olan NACA 0010 tercih edilmiştir. Profil seçiminin ardından konfigürasyon aşamasında kanat, gövde, kuyruk ve iniş takımı konfigürasyonları yapılmıştır. Hava aracının daha dengeli ve kararlı olmasını sağlamak için ortadan kanat ve T kuyruk tercih edilirken parazit sürükleme ve radar görünürlüğünü azaltmak için ise geleneksel gövde ve gövde içine alınabilen iniş takımı tercih edilmiştir. Uygun konfigürasyonların belirlenmesinden sonra aerodinamik ve kontrol yüzeylerinin boyutlandırılması yapılarak hava aracının 3 boyutlu CAD çizimi oluşturulmuştur. Faydalı yük olarak hava aracını güvenli bir şekilde kaldırabilecek ve görevin sorunsuz bir şekilde tamamlanmasını sağlayacak güce sahip fırçasız T-Motor MN4014 , motora uyumlu olarak 40A akım kapasitesine sahip ESC, 4S 5000mAh Li-Po batarya ve gece/gündüz keşif görevlerinde kötü hava şartlarında dahi görüntüleme yeteneğine sahip Teledyne FLIR hadron 640 görüntüleme sistemi tercih edilmiştir. Bu tasarım günümüz savunma alanındaki ihtiyaçları karşılamak açısından önemli bir katkı sağlamaktadır. Tasarım aşaması tamamlandıktan sonra hava aracının boylamasına kararlılığının incelenmesi adına durum uzay matrisleri oluşturulmuştur. Matris içerisinde bulunan değerler XFLR5 yazılımı aracılığıyla kararlılık analizleri sonucunda elde edilirken matriste bulunan elevatör sapma açısı OpenVSP yazılımı aracılığıyla elde edilmiştir. Son olarak kararlığın incelenmesi amacıyla PID kontrolcüleri kullanılarak en iyi sistem cevabı elde edilmiştir.

To cite this article:
Çınar, Z., Uzun, R., Dağ, T., & Oktay, T. (2025). Design and Longitudinal Stability Analysis of a Stealth Unmanned Aerial Vehicle. Aerospace Research Letters (ASREL), 4(2), 153-167.

***Corresponding Author:** Rabia Uzun, *ra.rabia8@gmail.com*

INTRODUCTION

Today, unmanned aerial vehicles are used in many areas, primarily in the military field. It is very important that unmanned aerial vehicles are designed to suit the task they are assigned. Traffic control, attacking enemy forces, border surveillance, gathering intelligence by infiltrating enemy lines, measuring air pollution, etc., are some of these tasks, and the aircraft designed for each task must be specific to that task (DAĞ et al., 2022; Nikolaou et al., 2025). For example, it is of great importance that unmanned aerial vehicles used in reconnaissance, surveillance, and intelligence gathering missions can continue their operations without being detected by enemy radar systems. At this point, stealth technology comes to the fore. The concept of stealth encompasses various design and material characteristics that make it difficult for an aircraft to be detected by enemy radars. The first aircraft designed and manufactured using this technology was the F-117A Nighthawk. The F-117 is an aircraft designed by Lockheed Martin to attack high-value targets without being detected by enemy radar and to carry out precision strikes (Ashraf et al., 2018).

The aircraft designed in this study is intended to gather information by conducting surveillance without being detected by enemy radar. Low visibility, which prevents detection by enemy radar, is a crucial technology for the designed aircraft. This feature is also related to the aircraft's aerodynamic structure and stability characteristics. Stability refers to the aircraft's ability to maintain flight without pilot intervention. Stability for an aircraft is examined in two ways: Longitudinal stability and lateral stability. In this study, longitudinal stability criteria were considered with the aim of ensuring the aircraft's safe flight (Dündar et al., 2020). Longitudinal stability controls the aircraft's nose-up or nose-down movements, while lateral stability controls the aircraft's right-left turns. When examining longitudinal stability, the most important part is the control surface, i.e., the elevator, located on the horizontal tail. The elevators located on the horizontal tail move in the same direction to maintain moment equilibrium. There are two control surfaces that affect lateral stability: the rudder located on the vertical tail and the ailerons located on the wings (Çopur et al., 2025). The ailerons are placed at the tips of both wings. The reason for this is to ensure maximum effectiveness when turning the aircraft. The two ailerons move in opposite directions to provide the turning motion.

In this study, the design of a 10 kg mini unmanned aerial vehicle was completed with a focus on low visibility for observation purposes. Subsequently, the longitudinal stability of this aerial vehicle was examined and the necessary assessments were made.

METHOD

In this section of the study, payloads were determined, configurations were selected, and the aircraft was sized. Table 1 lists the desired design requirements for the designed aircraft.

Table 1
Design Requirements

Requirement	Value
Cruise Speed	30 m/s
Stall Speed	27 m/s
Maximum Altitude	1000 m
Maximum Weight	10 kg

Payloads

One of the factors affecting the successful completion of an aircraft's mission is its power and propulsion systems. This system consists of the motor, electronic speed controller, and battery used as the energy source. In this study, the brushless T-Motor MN4014 was selected for a mini unmanned aerial vehicle with a takeoff weight of 10 kg. An ESC with a 40A current capacity compatible with the motor was selected. The selected ESC was determined according to the motor's operating voltage and maximum current. A 4S 5000mAh Li-Po battery was chosen as the energy source, and the Teledyne FLIR Hadron™ 640, which is high-resolution and capable of imaging even in adverse weather conditions, was selected as the imaging system.

Material Selection

In stealth technology, material selection is important in terms of reducing the radar cross-section and minimizing the reflection of electromagnetic waves. For this reason, radar-absorbing materials and composite materials are generally used. In this study, carbon fiber reinforced polymers were also preferred due to their high strength-to-weight ratio and ability to absorb radar waves (Srikar et al., 2025).

Configuration Selection

In this section, the wing, fuselage, tail, and landing gear configurations for the aircraft have been designed separately.

Wing Configuration

One of the elements that most affects aerodynamic efficiency in the design phase of unmanned aerial vehicles is wing profiles. Therefore, during the design phase, five different wing profiles were analyzed in terms of criteria such as lift coefficient, drag coefficient, and moment coefficient. The Reynolds number used in the analyses was calculated as 310329 using Equation 1. The Mach number was calculated as 0.090 using Equation 2 (DAĞ et al., 2023; Løw-Hansen et al., 2025).

v: Fluid velocity

ρ: Fluid density

υ: Fluid kinetic viscosity

μ: Fluid dynamic viscosity

l: Characteristic length of the profile

$$\mathrm{Re} = \frac{\rho v l}{\mu} \qquad (1)$$

$$M = \frac{V}{a} \qquad (2)$$

In this study, the DEA-51, E387, S1210, NACA 1412, and WORTMANN airfoil profiles were analyzed according to the specified criteria. During the evaluation process, the maximum lift coefficient $(CL)_{max}$, minimum drag coefficient $(CD)_{min}$, and moment coefficient $(CM)_0$ were considered, and a decision matrix was created in Table 2 based on these parameters. The obtained XFLR5 analysis results are shown in Figure 1, Figure 2, and Figure 3.

Table 2
Wing Profile Configuration

Profil	$(C_L)_{max}$	$(C_D)_{min}$	$(C_M)_0$
DAE-51	1.3	0.009	-0.11
E387	1.2	0.008	-0.09
NACA 1412	1.1	0.008	-0.07
S1210	1.9	0.012	-0.25
Wortmann FX 63-137	1.7	0.011	-0.20

Figure 1
Cl-Alpha graph

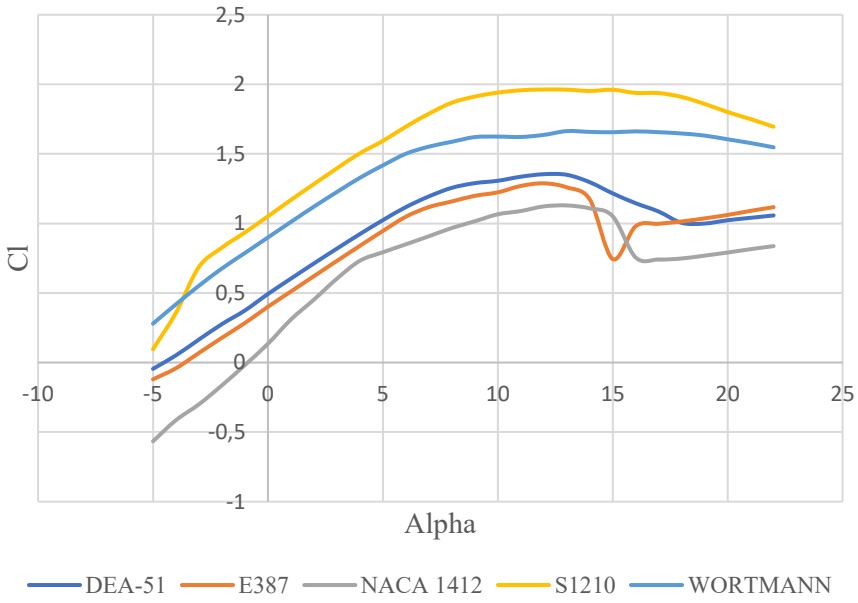

Figure 2
Cd-Alpha graph

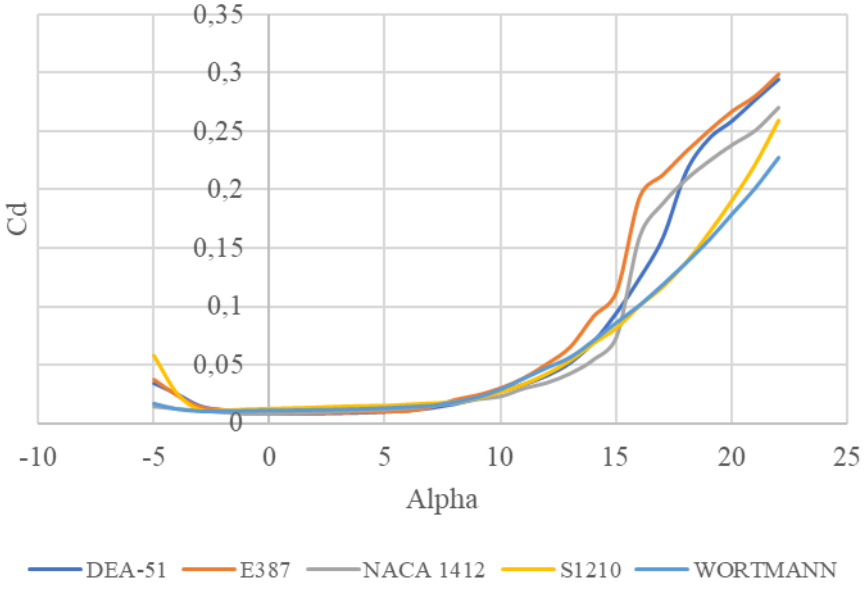

Figure 3

Cm-Alpha graph

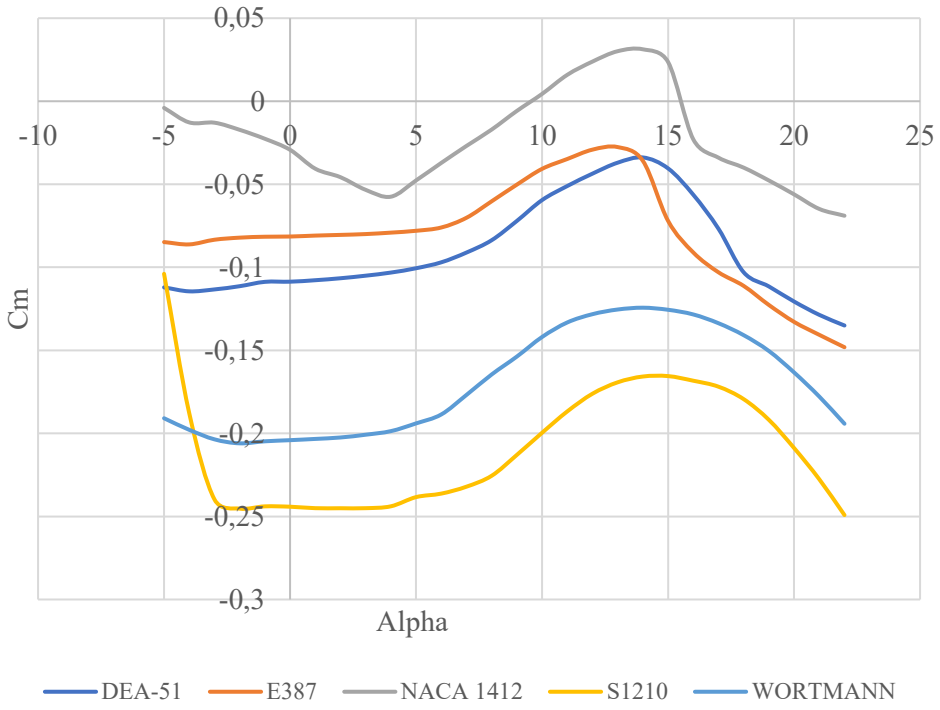

The analysis revealed that the S1210 wing profile has a higher lift coefficient than other profiles, produces low drag force at low angles of attack, and tends to return the aircraft to a balanced state due to its negative moment coefficient. Based on these characteristics, the S1210 was selected as the most suitable wing profile for this study.

After selecting the wing profile, the wing position was determined. The top, center, and bottom wing configurations were evaluated based on weight, stability, aerodynamic efficiency, radar visibility, and manufacturability criteria, and Table 3 was created.

Table 3

Wing Configuration

Criteria	Score Percentage	High Wing	Mid Wing	Low Wing
Weight	20%	3	4	5
Stability	30%	4	5	2
Aerodynamic Efficiency	20%	5	4	3
Radar Visibility	20%	2	3	4
Manufacturability	10%	3	4	2
Total	100%	3.5	4.1	3.2

As a result of the evaluation, a mid-wing configuration was selected in this study to ensure greater balance and stability of the aircraft.

Fuselage Configuration

The fuselage configuration selection was made from among the traditional fuselage, wing profile fuselage, and box fuselage, taking into account weight, drag, radar visibility, and stability criteria, as shown in Table 4.

Table 4

Fuselage Configuration

Criteria	Score Percentage	Traditional Fuselage	Drop Fuselage	Box Fuselage
Stability	30%	5	3	4
Radar Visibility	30%	3	4	1
Weight	25%	5	3	2
Parasite Drag	15%	3	5	1
Total	100%	4.1	3.6	2.15

Among the important parameters of the designed aircraft, its radar visibility,stealth capability, is noteworthy. Since the aircraft's longitudinal stability will be examined, stability is another parameter of high importance in addition to this feature. In body comparisons, these criteria are met by traditional and teardrop bodies. On the other hand, the box fuselage, due to its angular and transitional structure between surfaces, produces parasitic drag and is also a fuselage type that is unfavorable in terms of radar visibility. As a result of the evaluations, it was decided to use the traditional fuselage as the fuselage type in this design.

Tail Configuration

When configuring the tail, the tail profile was selected first. When selecting the tail profile, it was determined that cambered profiles were not suitable for the designed aircraft because they create unnecessary moments and additional drag forces. Since the goal was to produce these symmetrical aerodynamic responses on both sides of the tail surfaces, the symmetrical NACA 0010 profile was chosen for this study, and the analysis results obtained using the XFLR5 software are shown in Figures 4 and 5.

Figure 4

Cl-Alpha Graph

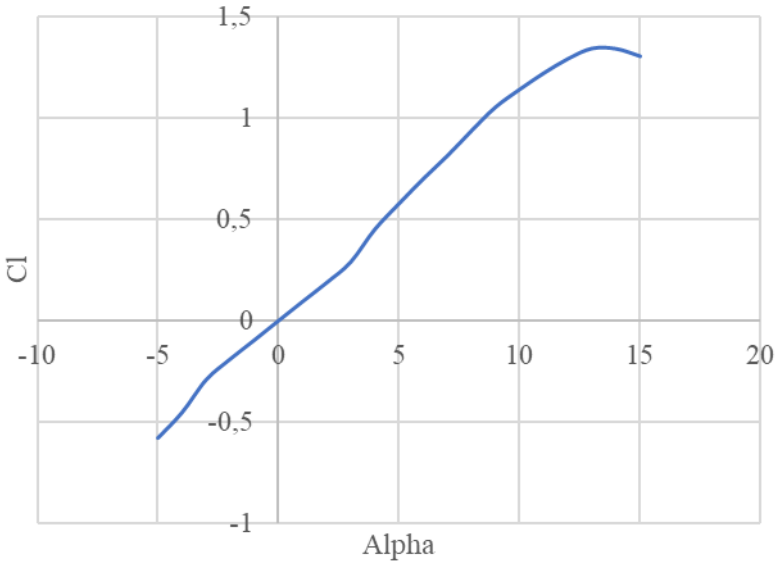

Figure 5
Cd-Alpha Graph

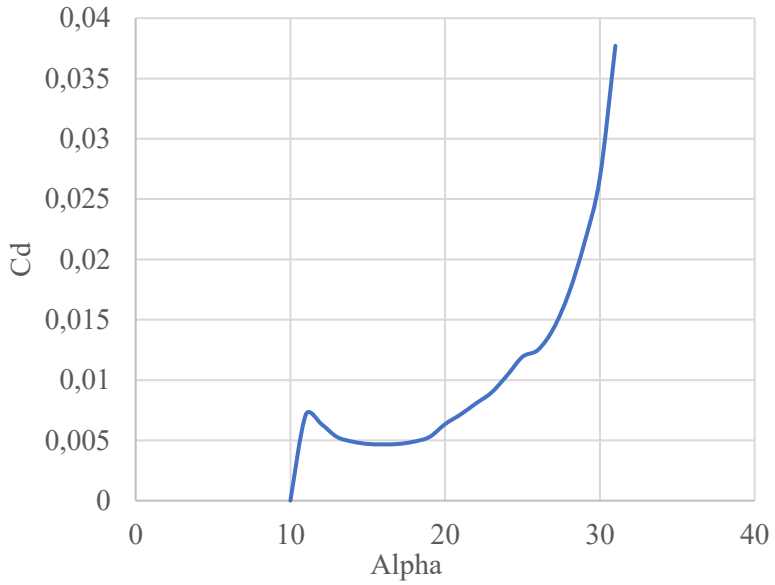

After selecting the queue profile, the queue type was selected and is specified in Table 5.

Tablo 5
Tail Configuration

Criteria	Score Percentage	H Tail	Traditional Tail	T Tail	V Tail
Radar Visibility	20%	2	2	2	3
Stability	20%	5	4	5	4
Equilibrium	20%	5	4	5	4
Parasite Drag	15%	2	3	3	3
Weight	15%	2	4	3	3
Producibility	10%	3	5	3	3
Total	100%	3.3	3.55	3.6	3.4

Tail types were compared based on six parameters, primarily stability, radar visibility, and balance. Since the aircraft will undertake observation tasks, factors affecting observation capability, such as camera and other technical component vibrations, should be minimized; therefore, balance and vehicle stability are crucial parameters. When examining Table 3, the H tail and T tail stand out among the compared tail types in this regard. When compared based on parasitic drag and weight parameters, the T tail was selected as the best tail type among these two.

Landing Gear Configuration

When selecting landing gear for the designed aircraft, fixed landing gear was not preferred because it produces extra parasitic drag and creates a sharp line on the aircraft, thereby increasing its radar visibility. Instead, retractable landing gear that can be retracted into the fuselage was preferred.

Sizing

In this section, the dimensions of the aircraft's wing, fuselage, tail, and control surface elements were determined individually.

Wing Sizing

Wings are the component that enables aircraft to remain airborne by generating lift during flight. Considering the mission requirements, the CL value was determined as 1.56328 for this aircraft design, which will operate at a takeoff weight of 10 kg, a cruise speed of 30 m/s, and a 4-degree angle of attack. Using all these data in Equation 3, the wing area of the aircraft was calculated as 0.1254 m².

$$L = W = \frac{1}{2} p_{\infty} * V_{\infty}^2 * S * C_L \qquad (3)$$

After calculating the wing area, the AR value was taken as 5.10 based on Raymer's recommendations, and the wing span was calculated as 0.8 m using Equation 4. A straight wing was chosen, and the tip and root chord values were calculated as 0.1667 m using Equation 5. Finally, the average aerodynamic chord was calculated as 0.1667 m using Equation 6 (Raymer, 1989).

$$AR = \frac{b^2}{S} \qquad (4)$$

$$S = \frac{b(C_{root} + C_{tip})}{2} \qquad (5)$$

$$MAC = \frac{2}{3} c_{root} \frac{(1+\lambda+\lambda^2)}{(1+\lambda)} \qquad (6)$$

Fuselage Sizing

When sizing the fuselage, consideration was given to the aircraft's ability to carry the equipment necessary for the specified operation. If the fuselage length is chosen to be too short, instability and balance issues will arise in the aircraft. If the fuselage length is chosen to be too long, unnecessary weight and increased parasitic drag will occur depending on the length. For this reason, it is very important that the fuselage has the appropriate dimensions for the necessary equipment. Taking all these considerations into account, the fuselage length has been determined to be 0.528 m.

$$l_f = b_w \times \frac{66}{100} \qquad (7)$$

Tail Sizing

During the selection of the aircraft's tail configuration, it was decided to use a T-tail as the tail type. When calculating the dimensions of this tail, the horizontal and vertical tails will be dimensioned separately, but the same procedure will be followed. First, Raymer's recommendations for determining the tail length based on the fuselage length were taken into account, and the tail lengths were calculated to be 60% of the fuselage. Equation 8 was used during the calculations, and the values of l_{HT} and l_{VT} were found to be 0.316 m.

$$l_{HT} = l_{VT} = l_f \times \frac{60}{100} \qquad (8)$$

Subsequently, Equations 9 and 10 were used to determine the horizontal and vertical tail areas, and calculations were performed by accepting the C_{HT} and C_{VT} values in the equations as 0.5 and 0.04, respectively, taking into account Raymer's recommendations for horizontal and vertical tail volume ratios. Subsequently, the S_{HT} and S_{VT} values were obtained as 0.0351 m² and 0.012 m², respectively.

$$C_{HT} = \frac{S_{HT} \cdot l_{HT}}{S_w \cdot c_{mac}} \qquad (9)$$

$$C_{VT} = \frac{S_{VT} \cdot l_{VT}}{S_w \cdot b_w} \qquad (10)$$

Equation 11 was used to calculate the tail gaps, and the AR values in the equation were determined as 4 for the horizontal tail and 1.6 for the vertical tail, taking Raymer's recommendations into account. The gap value for the horizontal tail is 0.375 m, while for the vertical tail it is 0.138 m.

$$AR = \frac{b^2}{S} \qquad (11)$$

Finally, using Equation 12 to calculate the tail veter lengths, the CHT and CVT values were calculated as 0.094 m and 0.086 m, respectively.

$$S = b \times c \qquad (12)$$

Control Surfaces Sizing

Control surfaces are elements that enable the aircraft's movement along various axes. Those located on the wing are ailerons and enable the aircraft's turning movement. The surface element located on the horizontal tail is the elevator and enables the aircraft's nose-up movement. The vertical tail has a control surface called the rudder, which controls the nose's left and right movement. In some tail types where the horizontal and vertical tails are integrated, a combined control surface called a ruddervator, which combines the elevator and rudder, is used. Since a T-tail was used in this study, the elevator and rudder were sized separately. Control surfaces that are too large cause excessive sensitivity and instability, while those that are too small may not produce sufficient moment and may be ineffective at low speeds. For this reason, when designing the control surface elements, care was taken to ensure that they were neither too large nor too small. The percentage of the area and opening of the surface where the control surfaces are located, the percentage of the area and opening of the control element, and the area of the control element are tabulated and presented in Table 6. Furthermore, the flap value given in the table is valid for one flap. When calculating for both, the result can be obtained by multiplying by two.

Table 6
Control Surfaces Sizing

Control Surface	Veter Percentage	Span Percentage	Veter Value	Span Value	Area
Aileron	30%	50%	0.050 m	0.2 m	0.01 m^2
Elevator	32%	84%	0.028 m	0.30 m	0.0084 m^2
Rudder	35%	85%	0.030 m	0.116 m	0.0034 m^2

After the design and sizing of the aircraft were completed, the wing and tail dimensions were provided using Table 7.

Table 7
Wing and Tail Sizing

Features	Wing	Vertical Tail	Horizontal Tail
Area	0.1254 m^2	0.012 m^2	0.0351 m^2
Span	0.8 m	0.138 m	0.375 m
Aspect Ratio	5.10	1.6	4
Tip Veter	0.1667 m	0.086 m	0.094 m
Root Veter	0.1667 m	0.086 m	0.094 m
Taper Ratio	0	0	0

After the sizing of the aircraft was completed, a 3D drawing was created using CAD software, and an isometric view was provided using Figure 6.

Figure 6
Isometric View of the Aircraft

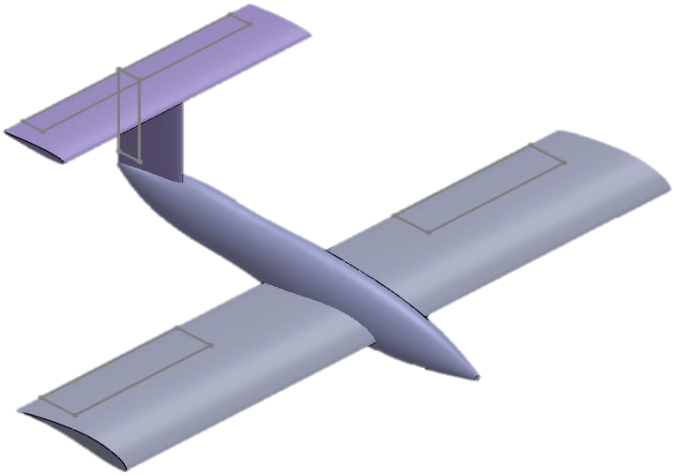

FINDINGS

This section will examine the longitudinal stability of the designed aircraft, which is the main objective of this study, by evaluating the system response after creating the state space matrices.

Investigation of Longitudinal Stability

The directions of the aircraft's axial movements, namely pitching, rolling, and yawing, have been reversed in this study. For this reason, the aircraft does not respond to stability assessment when the KP, KI, and KD values are positive (Çoban, 2024). As a result, when examining longitudinal stability, the KP, KI, and KD values will be selected as negative. First, the stability study was initiated with the standard values of KP=-50, KI =-5, and KD =-50. The system response is shown in Figure 7 (Bertran et al., 2022; Ma et al., 2025; Uzun et al., 2024).

Figure 7
Initial Longitudinal Stability Plot

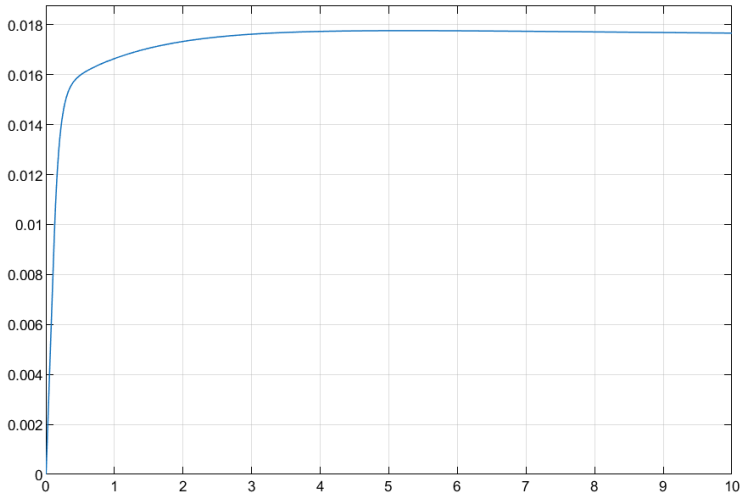

After examining Figure 7, it was decided to increase the KP value based on the general principles of PID improvement aimed at reducing steady-state error. However, since the axes of the designed aircraft were set in the negative direction, the KP value was decreased instead of increased, and the new graph created was examined using Figure 8 (KÖPRÜCÜ & ÖZTÜRK, 2024; Mien et al., 2024).

Figure 8
Longitudinal Stability Chart for Condition 2

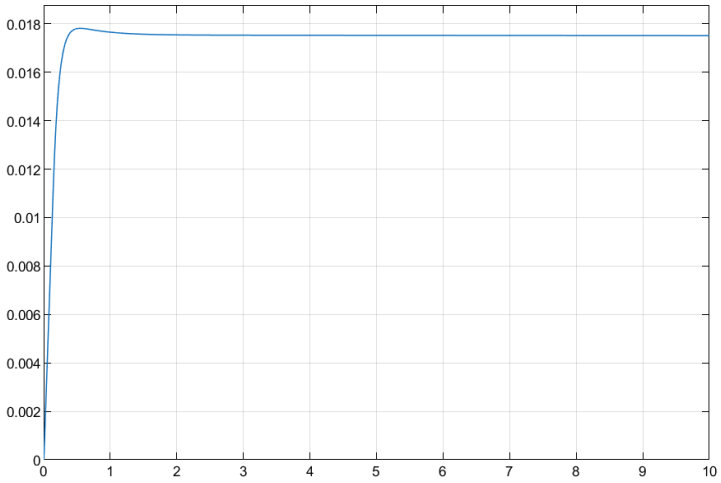

Subsequently, it was decided to reduce the K_D value to decrease the maximum overshoot obtained in the graph for the second case. Here again, the general principles are geared towards increasing the K_D value. In Figure 9, the K_D controller was improved and the new case was examined.

Figure 9
Longitudinal Stability Chart for Condition 3

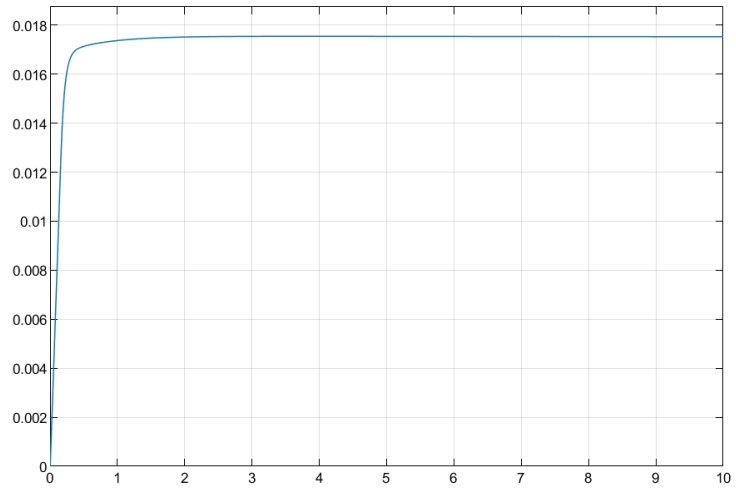

The system response obtained in Figure 9 is still insufficient in terms of stability. Therefore, the KP value has been reduced to improve the rise time. The KD values were reduced to improve the maximum overshoot. As a result of these improvements in the KP and KD values, the most stable state of the system was obtained. Since the axes of the designed vehicle are positioned in the negative direction, the KP and KD values were again accepted in a manner contrary to the general principles. Figure 10 shows the stable state of the system.

Figure 10

Longitudinal Stability Chart for the Most Stable Condition

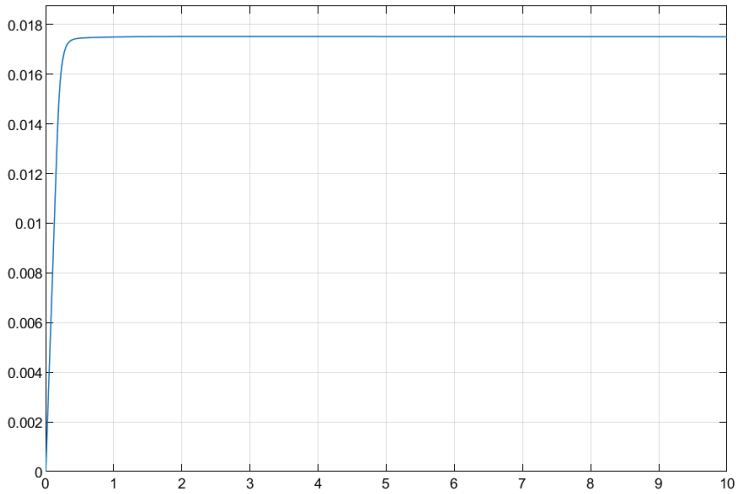

The K_I value is typically used to improve the system's rise time. In this study, the most stable state shown in Figure 10 was obtained while the K_I value remained unchanged at its standard value.

DISCUSSION AND RECOMMENDATIONS

The PID values obtained as a result of the stability study indicate that the aircraft is longitudinally stable. The required PID values were found using trial and error and were sufficient for this study. However, if a more stable condition is desired, various artificial intelligence techniques can be used (Uzun, 2024). In addition, the material used for stealth in the design phase was determined according to the weight of the designed aircraft and was effective in avoiding detection by radar. If extra stealth is desired, heavier and more effective materials can also be preferred; accordingly, the wing area or propulsion system that will provide the air vehicle's lifting force should be preferred. Furthermore, since the designed air vehicle was designed to be suitable for the mini jet UAV category, it can carry ammunition as a payload and attack enemy routes.

RESULTS

As a result of the studies conducted, the design of a fixed-wing unmanned aerial vehicle compliant with stealth technology and its 3D engineering model were created, and its longitudinal stability was examined.

• To enable the designed aircraft to successfully perform its mission, a brushless T-Motor MN4014, an ESC with a 40A current capacity, and a 4S 5000mAh Li-Po battery were used as the power and propulsion system, while the Teledyne FLIR Hadron™ 640 was chosen for the imaging system.

• A mid-wing configuration was chosen for the designed aircraft, with the S1210 wing profile selected. The aircraft wing has a span of 0.8 m and a wing area of 0.1254 m².

• A conventional fuselage was chosen for the designed aircraft, and the fuselage of this aircraft is 0.528 m long.

• The tail type used in the designed aircraft is a T-tail, and the NACA 0010 wing profile was chosen for the tail. The horizontal and vertical tail dimensions were determined separately. The vertical tail has a length of 0.138 m and an area of 0.012 m², while the horizontal tail has a length of 0.375 m and a tail area of 0.0351 m².

• The dimensioning of surface elements is a crucial point for the aircraft whose longitudinal stability will be examined. The winglet area of the UAV is 0.01 m², the elevator area is 0.0084 m², and the rudder area is 0.0034 m².

Calculations and analyses have determined that the aircraft possesses aerodynamic characteristics suitable for flight. While examining the aircraft's stability, the K_P, K_I, and K_D control coefficients were optimized by increasing and decreasing them. Longitudinal stability analyses have demonstrated that the aircraft exhibits safe flight performance.

Yazarlık Katkıları

Tasarım/Design: Zekiye ÇİNAR (50%) – Rabia UZUN (50%)

Veri Toplama veya veri girişi yapma/Data Collection or Processing: Rabia UZUN (50%) – Zekiye ÇİNAR (50%)

Analiz ve yorum/Analysis or Interpretation: Zekiye ÇİNAR (40%) – Rabia UZUN (40%) – Tolunay DAĞ (10%) – Tuğrul OKTAY (10%)

Literatür tarama/Literature Search: Rabia UZUN (50%) – Zekiye ÇİNAR (50%)

Yazma/Writing: Zekiye ÇİNAR (40%) – Rabia UZUN (40%) – Tolunay DAĞ (10%) – Tuğrul OKTAY (10%)

Finance

Finansal destek yoktur

Conflict of Interest

Çıkar çatışması yoktur.

REFERENCES

Ashraf, R., Tabassum, S. T., Tahmid, R., & Hossam-E-Haider, M. (2018). Performance Analysis of Radar Cross Section for F-117 Nighthawk Stealth Aircraft over Frequency and Aspect Angle. *2018 International Conference on Computer, Communication, Chemical, Material and Electronic Engineering (IC4ME2)*, 1–4. https://doi.org/10.1109/IC4ME2.2018.8465587

Bertran, E., Tercero, P., & Sànchez-Cerdà, A. (2022). UAV generalized longitudinal model for autopilot controller designs. *Aircraft Engineering and Aerospace Technology*, *94*(3), 380–391. https://doi.org/10.1108/AEAT-08-2020-0156

Çoban, S. (2024). Stochastic redesign of mini UAV wing for maximizing autonomous flight performance. *Aircraft Engineering and Aerospace Technology*, *96*(1), 113–120. https://doi.org/10.1108/AEAT-03-2023-0061

Çopur, E. H., Balta, E., & Bilgic, H. H. (2025). Tuning of cascade PID controller gains of quadcopter under bounded disturbances using metaheuristic based research algorithm. *The Aeronautical Journal*, *129*(1337), 1810–1832. https://doi.org/10.1017/aer.2025.12

DAĞ, T., ÜNLER, T., ÇOPUR, E. H., & ÇAKIN, U. (2022). Kentsel Hava Taşımacılığında Kullanılacak Dikey İniş-Kalkış Kabiliyetine Sahip Bir Hava Aracının Kavramsal Tasarımı ve Menzil Hesabı. *Konya Journal of Engineering Sciences*, *10*(3), 649–664. https://doi.org/10.36306/konjes.1090492

DAĞ, T., ÜNLER, T., & UYANER, M. (2023). Elektrikli İnsansız Hava Aracının Maksimum Menzil Hesabı. *ASREL*. https://doi.org/10.56753/ASREL.2023.1.2

Dündar, Ö., Bilici, M., & Ünler, T. (2020). Design and performance analyses of a fixed wing battery VTOL UAV. *Engineering Science and Technology, an International Journal*, *23*(5), 1182–1193. https://doi.org/10.1016/j.jestch.2020.02.002

KÖPRÜCÜ, S., & ÖZTÜRK, M. (2024). Comparison of PID Coefficients Determination Methods for Aircraft Pitch Angle Control. *ASREL*. https://doi.org/10.56753/ASREL.2024.3.5

Løw-Hansen, B., Hann, R., Gryte, K., Johansen, T. A., & Deiler, C. (2025). Modeling and identification of a small fixed-wing UAV using estimated aerodynamic angles. *CEAS Aeronautical Journal*, *16*(2), 501–523. https://doi.org/10.1007/s13272-025-00816-3

Ma, H., Zhou, Z., & Zhang, D. (2025). Control Characteristics Analysis of Multi-Section Morphing Wing Based on Centroid Self-Trimming. *IEEE Access*, *13*, 12996–13014. https://doi.org/10.1109/ACCESS.2024.3519800

Mien, T. L., Tu, T. N., & An, V. Van. (2024). Cascade PID Control for Altitude and Angular Position Stabilization of 6-DOF UAV Quadcopter. *International Journal of Robotics and Control Systems*, *4*(2), 814–831. https://doi.org/10.31763/ijrcs.v4i2.1410

Nikolaou, E., Kilimtzidis, S., & Kostopoulos, V. (2025). Winglet Design for Aerodynamic and Performance Optimization of UAVs via Surrogate Modeling. *Aerospace*, *12*(1). https://doi.org/10.3390/aerospace12010036

Raymer, D. (1989). *Aircraft Design-A Conceptual Approach*. AIAA Education.

Srikar, H. S., Hariharan, A., Manikandan, K., & Arul Jeya Kumar, A. (2025). Mechanical and electromagnetic absorption study on polyaniline and graphene oxide filled epoxy reinforced with graphite-carbon plate composites for stealth application. *Polymer Composites*, *46*(1), 412–426. https://doi.org/10.1002/pc.28996

Uzun, M. (2024). Flight control system design of UAV with wing incidence angle simultaneously and stochastically varied. *Aircraft Engineering and Aerospace Technology*, *96*(5), 715–725. https://doi.org/10.1108/AEAT-11-2023-0287

Uzun, M., Bilgic, H. H., Çopur, E. H., & Çoban, S. (2024). The aerodynamic force estimation of a swept-wing UAV using ANFIS based on metaheuristic algorithms. *Aeronautical Journal*,

128(1322), 739–755. https://doi.org/10.1017/aer.2023.73